Journal of Modern Optics

ISSN: 0950-0340 (Print) 1362-3044 (Online) Journal homepage: http://www.tandfonline.com/loi/tmop20

A comparative study of the optical and circuit representation of the unambiguous quantum state discriminator

Maritza Hernandez , Miguel Orszag & János A. Bergou

To cite this article: Maritza Hernandez , Miguel Orszag & János A. Bergou (2010) A comparative study of the optical and circuit representation of the unambiguous quantum state discriminator, Journal of Modern Optics, 57:3, 181-187, DOI: 10.1080/09500340903184329

To link to this article: http://dx.doi.org/10.1080/09500340903184329

Published online: 19 Aug 2009.

Journal of Modern Optics
Vol. 57, No. 3, 10 February 2010, 181–187

Taylor & Francis
Taylor & Francis Group

A comparative study of the optical and circuit representation of the unambiguous quantum state discriminator

Maritza Hernandez[a], Miguel Orszag[a] and János A. Bergou[b]*

[a]*Facultad de Física, Pontificia Universidad Católica de Chile, Casilla 306, Santiago, Chile;*
[b]*Department of Physics and Astronomy, Hunter College, City University of New York, 695 Park Avenue, New York 10065, USA*

(*Received 15 June 2009; final version received 14 July 2009*)

We propose a quantum circuit implementation of the unambiguous quantum state discriminator. The circuit is made entirely of standard logical quantum gates, and provides an optimal implementation of the Positive Operator Valued Measurement (POVM) for the unambiguous discrimination of quantum states. We also propose an actual experimental setup of this device using the vibrational degrees of freedom of one- or two-dimensional ion traps. We compare this implementation to the one that has been used exclusively so far in experiments, which is based on single-photon interferometry, and discuss their relative advantages.

Keywords: state discrimination; quantum circuits; ion trap quantum computing; linear optical implementation

1. Introduction

The discrimination of quantum states is a basic task in quantum information and quantum communication systems as well as in quantum cryptography [1]. A particularly clear example for the role of state discrimination in quantum cryptography is provided by the B92 QKD protocol [2]. A recent review on state discrimination can be found in [3]. Two popular strategies for optimal results are: the minimum error (ME) discrimination [4,5], where each measurement outcome selects one of the possible states and the error probability is minimized, and the unambiguous quantum state discrimination (USD) for linearly independent states [6], where we are not permitted to make an erroneous identification of the state, but we can get inconclusive results from the measurement. The goal is to minimize the fraction of the inconclusive results.

For the case of two pure states, with equal *a priori* probabilities, the optimum USD measurement was found more than a decade ago by Ivanovic [7], Dieks [8], and Peres [9]. The physical methods that have been previously proposed to implement USD include linear optical systems [10], ion trap architecture [11] and nuclear magnetic resonance [12]. In this work we shall deal with the unambiguous state discrimination, following the Peres model [9] and making use of POVM's for two known states. In particular, we propose a quantum circuit implementation of this device with logical quantum gates, and an experimental setup, employing trapped ions. We also investigate a different physical implementation which is based on single-photon optical interferometry and compare the relative strengths of these two different approaches.

The paper is organized as follows. In Section 2, we present the problem solved by Peres and the unitary operator U that can correlate the system under investigation to the probe. In Section 3, we show how to implement this unitary operator by means of CNOT and single-qubit unitary gates. In Section 4 we discuss the feasibility of the circuit implementation using trapped ions. In Section 5, we show an alternative implementation, in terms of optical interferometry and, finally, in Section 6 we provide a brief discussion and summary. Details of some of the calculations are presented in the Appendices.

2. Quantum discriminator

We want to discriminate unambiguously between two nonorthogonal states $|\Psi_0\rangle$ and $|\Psi_1\rangle$ that span a two-dimensional subspace of the complex Hilbert space.

$$|\Psi_0\rangle = a^{1/2}|0\rangle + (1-a)^{1/2}|1\rangle, \tag{1}$$

$$|\Psi_1\rangle = a^{1/2}|0\rangle - (1-a)^{1/2}|1\rangle, \tag{2}$$

where $a > \frac{1}{2}$.

*Corresponding author. Email: jbergou@hunter.cuny.edu

ISSN 0950–0340 print/ISSN 1362–3044 online

DOI: 10.1080/09500340903184329
http://www.informaworld.com

We consider an additional ancilla qubit in the state $|0\rangle$. The bases are labeled by A for the system and B for the ancilla. Our initial state is

$$|\Psi_i\rangle_{AB}^{\text{in}} = |\Psi_i\rangle_A \otimes |0\rangle_B = a^{1/2}|00\rangle_{AB} \pm (1-a)^{1/2}|10\rangle_{AB}, \quad (3)$$

where $\pm$ signs correspond to initial states $|\Psi_0\rangle_A$ and $|\Psi_1\rangle_A$, the second qubit is the ancilla, and $i=0, 1$.

Making use of the Peres choice, we define a unitary operator U that yields the following final state, when applied to $|\Psi_i\rangle_{AB}^{\text{in}}$

$$\begin{aligned}|\Psi_i\rangle_{AB}^{\text{out}} &= U_{AB}|\Psi_i\rangle_{AB}^{\text{in}} \\ &= (1-a)^{1/2}(|0\rangle_A \pm |1\rangle_A)|0\rangle_B \\ &+ (2a-1)^{1/2}|1\rangle_A|1\rangle_B \\ &= [2(1-a)]^{1/2}|\pm\rangle_A|0\rangle_B \\ &+ (2a-1)^{1/2}|1\rangle_A|1\rangle_B, \end{aligned} \quad (4)$$

where $|\pm\rangle_A \equiv (|0\rangle_A \pm |1\rangle_A)/2^{1/2}$.

If we perform a measurement on the ancilla (system B) and get the state $|0\rangle_B$, we can make a further von Neumann measurement on system A and unambiguously determine the input state. If the final state is the $|+\rangle_A$ state, then $|\Psi_i\rangle_A^{\text{in}} = |\Psi_0\rangle$, and if the final state is $|-\rangle_A$ state, then $|\Psi_i\rangle_A^{\text{in}} = |\Psi_1\rangle$, and the probability of the successful discrimination is $2(1-a) \equiv 1-\cos(2\theta)$. If the measurement on the ancilla gives the state $|1\rangle_B$, then the A qubit will always be in the state $|1\rangle_A$, so we get an inconclusive result with probability $2a-1 \equiv \cos(2\theta)$, where we introduced $a \equiv \cos^2(\theta)$.

We can write the unitary operator U_{AB}, in the basis $\{|00\rangle_{AB}, |01\rangle_{AB}, |10\rangle_{AB}, |11\rangle_{AB}\}$, as

$$U_{AB} = \begin{pmatrix} \left(\frac{1-a}{a}\right)^{1/2} & 0 & 0 & -\left(\frac{2a-1}{a}\right)^{1/2} \\ 0 & 1 & 0 & 0 \\ 0 & 0 & 1 & 0 \\ \left(\frac{2a-1}{a}\right)^{1/2} & 0 & 0 & \left(\frac{1-a}{a}\right)^{1/2} \end{pmatrix}. \quad (5)$$

In the next section we shall find a quantum circuit representation of this two-qubit unitary operator.

3. Implementation of U_{AB} in a quantum circuit

One of the main tools for the development of quantum computing is the construction of quantum circuits capable of realizing the processing and manipulation of the quantum information. In this context, it is necessary to decompose any unitary transformation in a sequence of quantum gates, resulting in a corresponding quantum circuit.

In this section, we review an algorithm to decompose an arbitrary unitary transformation $U \in SU(4)$ [13] in order to express the unitary transformation by a quantum circuit. Then we apply this procedure to the particular case of the unambiguous discriminator of known states (5).

3.1. Procedure to decompose a unitary matrix $U \in SU(4)$

The main decomposition is the Cartan decomposition [14], in the 'KAK' form from the Lie theory. Several cases have been studied, like the two-qubit *magic decomposition* [13,15–18], the *cosine-sine decomposition* [19–21], and the *demultiplexing decomposition* [21]. The first one is for two qubits, and the last two decompositions hold for n-qubit operators.

For any operator $U \in SU(4)$ (Figure 1) there exist local unitary operators U_A, U_B, V_A, V_B and a nonlocal unitary operator U_d such that

$$U = (U_A \otimes U_B)U_d(V_A \otimes V_B), \quad (6)$$

where

$$\begin{aligned} U_d &= \exp\left(-\mathrm{i}\overrightarrow{\sigma_A}^{\mathrm{T}} d \overrightarrow{\sigma_B}\right) \\ &= \exp\left[-\mathrm{i}(\alpha_x \sigma_x \otimes \sigma_x + \alpha_y \sigma_y \otimes \sigma_y + \alpha_z \sigma_z \otimes \sigma_z)\right] \\ &= \exp(-\mathrm{i}H). \end{aligned} \quad (7)$$

Here $\overrightarrow{\sigma}^{\mathrm{T}}$ is the transpose of Pauli operators denoted by $\overrightarrow{\sigma} = (\sigma_x, \sigma_y, \sigma_z)$ in the computational basis, $\{|0\rangle, |1\rangle\}$, the subscripts specify on which system the operator is acting, and d is a diagonal matrix whose diagonal elements are denoted by α_x, α_y, α_z. Due to the periodicity and symmetry of the entanglement generated by U_d one has the following restriction [13]:

$$\frac{\pi}{4} \geq \alpha_x \geq \alpha_y \geq |\alpha_z|. \quad (8)$$

It is easy to show that the operator U_d is diagonal in the magic basis $\{|\Phi_k\rangle\}$, defined as

$$\begin{aligned} |\Phi_1\rangle &= \frac{1}{2^{1/2}}(|00\rangle + |11\rangle), \quad |\Phi_2\rangle = \frac{\mathrm{i}}{2^{1/2}}(|00\rangle - |11\rangle), \\ |\Phi_3\rangle &= \frac{\mathrm{i}}{2^{1/2}}(|01\rangle + |10\rangle), \quad |\Phi_4\rangle = \frac{1}{2^{1/2}}(|01\rangle - |10\rangle). \end{aligned} \quad (9)$$

Therefore, U_d in the magic basis can be written as

$$U_d = \sum_{k=1}^{4} \exp(-\mathrm{i}\lambda_k)|\Phi_k\rangle\langle\Phi_k|, \quad (10)$$

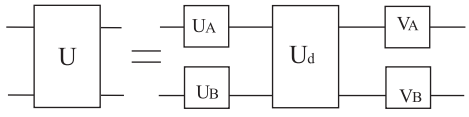

Figure 1. Decomposition of operator $U \in SU(4)$.

where the λ_k's are given by

$$\begin{aligned}\lambda_1 &= \alpha_x - \alpha_y + \alpha_z,\\ \lambda_2 &= -\alpha_x + \alpha_y + \alpha_z,\\ \lambda_3 &= \alpha_x + \alpha_y - \alpha_z,\\ \lambda_4 &= -\alpha_x - \alpha_y - \alpha_z.\end{aligned} \tag{11}$$

In order to find the matrices U_A, U_B, V_A, V_B and the phases λ_k in the decomposition (6), we follow the procedure given in [13].

The procedure goes as follows:

(a) Calculate U in the magic basis, then obtain the eigensystem of the product $U^{\mathrm{T}}U$, denoting the eigenvalues and eigenstates by $\exp(2\mathrm{i}\epsilon_k)$ and $|\Psi_k\rangle$, respectively.

(b) Following Lemma 1 of [13] (Appendix 1), choose V_A, V_B and the phases ξ_k, such that

$$V_A \otimes V_B \exp(\mathrm{i}\xi_k)|\Psi_k\rangle = |\Phi_k\rangle, \tag{12}$$

where $|\Psi_k\rangle$ corresponds to our eigenstates calculated in (a), and $|\Phi_k\rangle$ is the magic basis (9).

(c) According to the eigenvalues and eigenstates obtained in (a), calculate

$$\left|\widetilde{\Psi}_k\right\rangle = \exp(-\mathrm{i}\epsilon_k)U|\Psi_k\rangle. \tag{13}$$

(d) Using Lemma 1 again, choose the U_A, U_B and λ_k such that

$$U_A^{\dagger} \otimes U_B^{\dagger} \exp[\mathrm{i}(\lambda_k + \xi_k + \epsilon_k)]\left|\widetilde{\Psi}_k\right\rangle = |\Phi_k\rangle. \tag{14}$$

3.2. *Decomposition of the unitary matrix U_{AB}*

Following the above procedure, for our particular unitary matrix (5), we readily find the elements in the decomposition U_A, U_B, V_A, V_B (see Appendix 2):

$$\begin{aligned} V_A &= \begin{pmatrix} 1 & 0 \\ 0 & \exp\left(\frac{\mathrm{i}\pi}{4}\right)\end{pmatrix}, \quad V_B = \begin{pmatrix} 0 & 1 \\ \exp\left(-\frac{\mathrm{i}\pi}{4}\right) & 0\end{pmatrix},\\ U_A &= \begin{pmatrix} 1 & 0 \\ 0 & \exp\left(-\frac{\mathrm{i}\pi}{4}\right)\end{pmatrix}, \quad U_B = \begin{pmatrix} 0 & \exp\left(\frac{\mathrm{i}\pi}{4}\right) \\ 1 & 0\end{pmatrix},\end{aligned} \tag{15}$$

and the diagonal elements of U_d:

$$\begin{aligned}\exp(-\mathrm{i}\lambda_1) &= 1,\\ \exp(-\mathrm{i}\lambda_2) &= 1,\\ \exp(-\mathrm{i}\lambda_3) &= \left(\frac{1-a}{a}\right)^{1/2} - \mathrm{i}\left(\frac{2a-1}{a}\right)^{1/2},\\ \exp(-\mathrm{i}\lambda_4) &= \left(\frac{1-a}{a}\right)^{1/2} + \mathrm{i}\left(\frac{2a-1}{a}\right)^{1/2}.\end{aligned} \tag{16}$$

If we now compare Equations (11) and (16), we readily find $\alpha_z = 0$, $\alpha_x = \alpha_y \equiv \alpha$, and defining $\cos\phi = (1-a)^{1/2}/a^{1/2}$, we can write $\alpha = -\phi/2$, and $\exp(-\mathrm{i}\lambda_3) = \exp(2\mathrm{i}\alpha)$, $\exp(-\mathrm{i}\lambda_4) = \exp(-2\mathrm{i}\alpha)$.

We have all elements in decomposition (6), namely U_A, U_B, V_A, V_B and U_d. But we still can decompose U_d. Following [16], U_d can be further decomposed in terms of C-NOT and single qubit gates, as shown in Figure 2.

In the figure w is defined by

$$w = \frac{1 + \mathrm{i}\sigma_x}{2^{1/2}} = R_x(\pi/2) = \frac{1}{2^{1/2}}\begin{pmatrix} 1 & \mathrm{i} \\ \mathrm{i} & 1\end{pmatrix}, \tag{17}$$

and

$$\exp(-\mathrm{i}\alpha_x\sigma_x) = \exp(-\mathrm{i}\alpha\sigma_x) = \exp\left(\mathrm{i}\frac{\phi}{2}\sigma_x\right) = R_x(-\phi), \tag{18}$$

$$\exp(-\mathrm{i}\alpha_y\sigma_z) = \exp(-\mathrm{i}\alpha\sigma_z) = \exp\left(-\mathrm{i}\frac{\phi}{2}\sigma_z\right) = R_z(\phi). \tag{19}$$

Finally, the complete circuit for the unambiguous discriminator in terms of C-Not gates and single qubit rotations is shown in Figure 3. In Figure 3, $u_A = WV_A$ and $v_B = U_B W$.

Usually V_A is known as the $\pi/8$ gate (denoted T) [22]. Thus, $V_A = T = \exp(\mathrm{i}\pi/8)R_z(\pi/4)$, and $U_A = T^{\dagger} = \exp(-\mathrm{i}\pi/8)R_z(-\pi/4)$. On the other hand, U_B and V_B can also be represented as rotations, $V_B = \exp(-\mathrm{i}\pi/8)\times(\exp(\mathrm{i}\pi/2)R_x(\pi))R_z(\pi/4)$, $U_B = \exp(\mathrm{i}\pi/8)(\exp(\mathrm{i}\pi/2)R_x(\pi))R_z(\pi/4)$. Therefore, it is possible to write every single qubit operation as a product of rotations:

$$\begin{aligned} u_A &= \exp\left(\mathrm{i}\frac{\pi}{8}\right)R_z\left(\frac{\pi}{4}\right)R_x\left(\frac{-\pi}{2}\right),\\ v_B &= \exp\left(\mathrm{i}\frac{\pi}{8}\right)\exp\left(\mathrm{i}\frac{\pi}{2}\right)R_x(\pi)R_z\left(\frac{\pi}{4}\right)R_x\left(\frac{-\pi}{2}\right).\end{aligned} \tag{20}$$

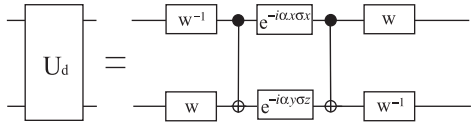

Figure 2. Quantum circuit for U_d in terms of a C-NOT and single qubit gates when $\alpha_z = 0$.

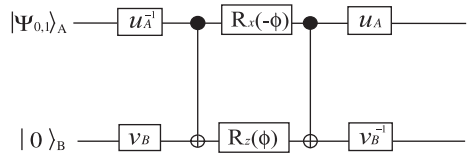

Figure 3. Complete quantum circuit for the unambiguous discriminator in terms of C-NOT gates and single qubit rotations.

4. Feasibility of the circuit implementation using trapped ions

The circuit proposed in the previous section uses several gates, namely, C-NOT gates and single qubit rotations. These gates can be implemented using, for example, trapped ions.

Single quantum bit operations for quantum information processing with trapped ions have been shown to be experimentally feasible, where individual addressing of single ions in a linear string with a laser beam is required [23]. Specifically, single-qubit rotations of trapped ion qubits have been implemented by turning laser beams on and off for a duration appropriate to achieve a certain rotation angle on the Bloch sphere. Arbitrary rotations on the Bloch sphere can be implemented by also controlling the relative phase of the laser beam, [24,25]. Cirac and Zoller were the first to propose the use of trapped ions for quantum computing in 1995, a two-qubit C-NOT gate, where a selected mode of motion is cooled to the ground state and the ground and first excited state of this mode are used as 'bus-qubit'. The spin qubit of an ion can be mapped onto the bus-qubit using a laser sharply focused onto that ion. In this way, a gate operation can be performed between the motional qubit and a second ion, thus effectively performing a C-NOT gate operation between the first and second ion.

On the other hand, Mølmer and Sørensen [26] also proposed a two-qubit gate, using two fields at different frequencies, which are non-resonant with the atomic transition, but when combined, produce a two-qubit transition. This scheme has certain advantages over the Cirac–Zoller scheme, namely, it consists of a one-step process and most importantly, it does not require individual ion–laser addressing, or in other words, both ions are equally illuminated.

The experimental realization of the Cirac–Zoller C-NOT gate was achieved by Schmidt-Kaler et al. in 2003 [27]. In their experiment, two $^{40}Ca^{+}$ ions are held in a linear Paul trap and are individually addressed using focused laser beams; the qubits are represented by superpositions of two long-lived electronic states.

5. Linear optical implementation

We obtain a very different physical implementation of the discriminator when we employ techniques from linear optical quantum interferometry combined with a generalization of the so-called dual-rail representation of a qubit (see [28,29]). The generalized measurement can then be realized by utilizing linear optical elements and photodetectors, based on the proposal of [30].

In order to accommodate the three possible returns from the optimal state discriminating measurement, we need a Hilbert space with a minimum dimensionality of three. We will span this Hilbert space by a single photon entering one of the three input ports of the six-port interferometer in Figure 4, so that the appropriate interferometer could be implemented for any desired discrimination problem.

The basis states of this interferometer, the so-called rails, are given by

$$\begin{aligned} |0\rangle_{AB} &= |100\rangle, \\ |1\rangle_{AB} &= |010\rangle, \\ |2\rangle_{AB} &= |001\rangle. \end{aligned} \tag{21}$$

Here a 1 in the first position refers to one photon entering the first port, while zero in the second and third position refers to vacuum entering the corresponding port, and similarly for the other states. With this representation the states to be discriminated, as given in Equations (1) and (2), can be expressed in terms of a single photon split between the first and second input ports. Thus, the first two ports represent the system, while the third port is always empty at the input and it serves as the ancilla. The subscript AB refers to the basis of the joint system–ancilla Hilbert space which is three-dimensional.

For the purposes of optical interferometry, we slightly modify the Peres choice to define a unitary operator U_{AB}, entangling the system with the ancilla.

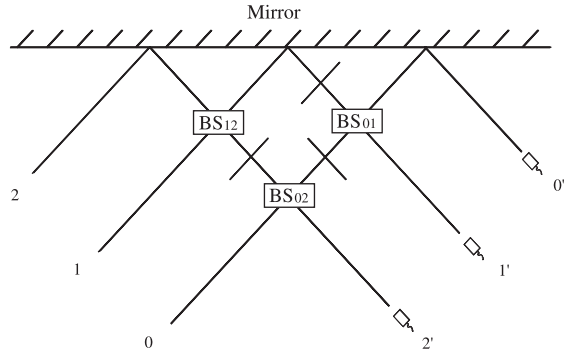

Figure 4. A general six-port optical interferometer. Suitable beamsplitters are placed at each crossing of two optical rails and suitable phase shifters (denoted by short lines crossing the corresponding rails) are placed at each internal arm before the beamsplitters to realize any desired 3×3 unitary transformation on the input states. To realize the optimal unambiguous discrimination of two known quantum states, i.e. to realize U_{AB} of Equation (23), only two beamsplitters are needed, BS_{02} and BS_{01}, with their parameters given in Equations (24) and (25). A detection in rail $2'$ corresponds to an inconclusive result and a detection in rails $0'$ (or $1'$) corresponds to state $|\psi_0\rangle$ (or $|\psi_1\rangle$).

It yields the following final state, when applied to $|\Psi_i\rangle_{AB}^{\text{in}}$ $(i=0,1)$,

$$\begin{aligned}|\psi_i\rangle_{AB}^{\text{out}} &= U_{AB}|\psi_i\rangle_{AB}^{\text{in}} \\ &= (2-2a)^{1/2}|i\rangle_{AB} + (2a-1)^{1/2}|2\rangle_{AB},\end{aligned} \tag{22}$$

where $|i\rangle_{AB}$ $(i=0,1)$ were defined in Equation (21).

Any $N\times N$-dimensional discrete unitary operation can be implemented by an appropriate multi-path optical interferometer, using beamsplitters and phase shifters only, as was shown in general in [31] and [32]. Based on this general result an all optical implementation was proposed in the particular context of state discrimination in [30]. We start by reviewing this proposal and address the actual determination and implementation of the unitary operator U_{AB}.

In the basis given by Equation (21) we have

$$U_{AB} = \begin{pmatrix} \left(\frac{1-a}{2a}\right)^{1/2} & \left(\frac{1}{2}\right)^{1/2} & \left(\frac{2a-1}{2a}\right)^{1/2} \\ \left(\frac{1-a}{2a}\right)^{1/2} & -\left(\frac{1}{2}\right)^{1/2} & \left(\frac{2a-1}{2a}\right)^{1/2} \\ \left(\frac{2a-1}{a}\right)^{1/2} & 0 & -\left(\frac{1-a}{a}\right)^{1/2} \end{pmatrix}. \tag{23}$$

The key point in the implementation of this unitary is the observation that it can be written as $U_{01}\,U_{02}$, where

$$U_{02} = \begin{pmatrix} \left(\frac{1-a}{a}\right)^{1/2} & 0 & \left(\frac{2a-1}{a}\right)^{1/2} \\ 0 & 1 & 0 \\ \left(\frac{2a-1}{a}\right)^{1/2} & 0 & -\left(\frac{1-a}{a}\right)^{1/2} \end{pmatrix}, \tag{24}$$

and

$$U_{01} = \begin{pmatrix} \left(\frac{1}{2}\right)^{1/2} & \left(\frac{1}{2}\right)^{1/2} & 0 \\ \left(\frac{1}{2}\right)^{1/2} & -\left(\frac{1}{2}\right)^{1/2} & 0 \\ 0 & 0 & 1 \end{pmatrix}. \tag{25}$$

Both of these unitaries correspond to beamsplitters. U_{02} is a beamsplitter placed at the intersection of beams 0 and 2 (BS_{02} in Figure 4) with a transmission coefficient of $t=[(1-a)/a]^{1/2}=\tan\theta$ and reflection coefficient of $r=[(2a-1)/a]^{1/2}=(1-\tan^2\theta)^{1/2}$. Thus, BS_{02} is related to the parameters of the input states in a very simple way. U_{01} is simply a 50 : 50 beamsplitter placed at the intersection of beams 0 and 1 (BS_{01} in Figure 4) with transmission and reflection coefficients of $t=r=1/2^{1/2}$. In fact, U_{02} is essentially identical to the unitary given in Equation (5) (after discarding the unused degree of freedom) and accomplishes the exact same task. The coefficient of the $|0\rangle$ state in both input states is the same, $a^{1/2}$. By transmitting only a portion of $[(1-a)/a]^{1/2}$ of the $|0\rangle$ state, the components of the two inputs that remain in the original system Hilbert space become orthogonal and transform into the $|\pm\rangle$ states, so they can, in principle be discriminated by standard von Neumann measurements. The role of the second beamsplitter is to transform the $|\pm\rangle$ states into the $|0\rangle$ and $|1\rangle$ states, respectively, so they can be discriminated by projective measurements in the computational basis. The third beamsplitter, BS_{12}, and the phase shifters are not needed in this implementation.

Now that we have seen how one can implement the above unitary with the six-port interferometer, we discuss how this implementation works. We can place single-photon detectors in each of the output ports of the six-port interferometer. If the detector at output port $0'$ clicks it unambiguously identifies the input as $|\Psi_0\rangle$, if the one at $1'$ clicks it identifies the input as $|\Psi_1\rangle$. The probability of the successful discrimination is $2(1-a)\equiv 1-\cos(2\theta)$, same as before. If the detector at $2'$ clicks the result is inconclusive. The probability of the inconclusive outcome is $2a-1\equiv\cos(2\theta)$, again same as before, so this is an implementation of the optimal POVM.

After the explanation of how this implementation performs, three remarks are in order here. First, there is a remarkable simplicity inherent in this implementation as it requires only two beamsplitters. Second, the implementation requires one extra dimension only, not two as the previous implementation, so it works in 3D. This could be an advantage (although it should be mentioned that qubit ancillas are very cheap and readily available on demand). The fact that this particular implementation requires one extra dimension only originates in the fact that optical elements can address individual degrees of freedom of the ancilla, of which only one is used. The third advantage of this particular implementation is that the final measurement is carried out in the computational basis and not in the $|\pm\rangle$ basis which is conceptually simpler and, in our rail representation, it corresponds to the detection of a single photon in the appropriate rail.

Thus, a single-photon representation of the input and output states, a multirail optical network (in our case a six-port) for performing the unitary transformation U_{SA}, Equation (23), and photodetectors at each of the output ports, to carry out the required nonunitary transformation, accomplish the required optimal discrimination task. For the case of two nonorthogonal states, $\{|\psi_0\rangle,\ |\psi_1\rangle\}$, living in a 2D Hilbert space, a six-port optical interferometer can be constructed to perform transformations in the 3D system plus ancilla space. All beamsplitters in this interferometer were designed to be optimal for given input states. By using beamsplitters to send one photon into some linear superposition of the first two rails, we can generate arbitrary quantum states in this two-dimensional Hilbert space, represented as $|\psi\rangle_{\text{in}}=\sum_{j=0}^{1} c_j|j\rangle$, where $\sum_{j=0}^{1}|c_j|^2=1$, and $|j\rangle$ is the jth optical rail state. Note that the third rail, which acts

as the ancilla, never contains a photon at the input. The interferometer is designed to perform the unitary operation U_{AB} which optimizes state discrimination. It maps the input states $|\psi_i\rangle$ into output states given by Equation (22). A photon in mode $2'$ now indicates an inconclusive result. On the other hand, a photon in rail $0'$ or $1'$ unambiguously indicates that the initial state was $|\psi_0\rangle$ or $|\psi_1\rangle$, respectively.

6. Discussion

Following Peres' [9] proposal for an unambiguous quantum discriminator of known states, we derived a four-dimensional unitary transformation and describe step by step an algorithm that converts the unitary into a quantum circuit involving only standard one- and two-qubit gates. We have shown how one can implement the discriminator in terms of trapped ions. Both the required C-NOT and single qubit rotation gates have been recently implemented, using ions in a linear trap, with the qubits corresponding to the atomic sublevels and the bus, in the case of the two-qubit gate, corresponding to a quantized vibrational motion state of the ions [24,27]. Furthermore, we have also discussed a linear optical implementation, using techniques of single-photon interferometry, that gives an alternative physical realization of the optimal discriminator. The circuit implementation uses readily available, off-the shelf elements only but the algorithm required to convert a given unitary into a quantum circuit can be quite involved and, even for a relatively simple task, the number of necessary elements can be quite large. The optical implementation, on the other hand, is conceptually much simpler for simple tasks and usually requires a few beamsplitters and phase shifters only. In fact, until now all experiments in this area have been based on some variant of the optical implementation [33]. This simplicity, however, can be quite misleading. The complexity of the multiport interferometer increases exponentially with the size of the problem and alignment of the beams as well as the number of optical elements make this implementation impractical for larger systems, whereas the complexity of the circuit implementation, being based on standard elements, will increase only polynomially with the size of the problem and becomes preferable for larger systems.

References

[1] Gisin, N.; Ribordy, G.; Tittel, W.; Zbinden, H. *Rev. Mod. Phys*. **2002,** *74,* 145–195.

[2] Bennett, C.H. *Phys. Rev. Lett*. **1992,** *68,* 3121–3124.

[3] Bergou, J.A.; Herzog, U.; Hillery, M. *Lecture Notes in Physics*; Springer: Berlin, 2004; Vol. 649, p 417.

[4] Helstrom, C.W. *Quantum Detection and Estimation Theory*; Academic Press: New York, 1976.

[5] Holevo, A.S. *Probabilistic and Quantum Aspects of Quantum Theory*; North-Holland: Amsterdam, 1982.

[6] Chefles, A. *Phys. Lett. A* **1998,** *239,* 339–347.

[7] Ivanovic, I.D. *Phys. Lett. A* **1987,** *123,* 257–259.

[8] Dieks, D. *Phys. Lett. A* **1988,** *126,* 303–306.

[9] Peres, A. *Phys. Lett. A* **1988,** *128,* 19.

[10] Bergou, J.A.; Hillery, M.; Sun, Y. *J. Mod. Opt*. **2000,** *47,* 487–497.

[11] Roa, L.; Retamal, J.C.; Saavedra, C. *Phys. Rev. A* **2003,** *66,* 012103.

[12] Gopinath, T.; Das, R.; Kumar, A. *Phys. Rev. A* **2005,** *71,* 042307.

[13] Kraus, B.; Cirac, J.I. *Phys. Rev. A* **2001,** *63,* 062309.

[14] Knapp, A.W. In *Lie Groups Beyond an Introduction*; Progress in Mathematics Series; Birkhäuser: Boston, 1996; Vol. 140.

[15] Makhlin, Yu.G. *QIP* **2002,** *1,* 243–252.

[16] Vidal, G.; Dawson, C.M. *Phys. Rev. A* **2004,** *69,* 010301(R).

[17] Shende, V.V.; Markov, I.L.; Bullock, S.S. *Phys. Rev. A* **2004,** *69,* 062321.

[18] Zhang, Y.S.; Ye, M.Y.; Guo, G.C. *Phys. Rev. A* **2005,** *71,* 062331.

[19] Khaneja, N.; Glaser, S.J. *J. Chem. Phys*. **2001,** *267,* 11–23.

[20] Möttönen, M.; Vartiainen, J.J.; Bergholm, V.; Salomaa, M.M. *Phys. Rev. Lett*. **2004,** *93,* 130502.

[21] Shende, V.V.; Bullock, S.S.; Markov, I.L. *IEEE Trans. CAD* **2006,** *25,* 1000–1010.

[22] Nielsen, M.A.; Chuang, I.L. *Quantum Computation and Quantum Information*; Cambridge University Press: Cambridge, UK, 2000.

[23] Nägerl, H.C.; Leibfried, D.; Rhode, H.; Thalhammer, G.; Eschner, J.; Schmidt-Kaler, F.; Blatt, R. *Phys. Rev. A* **1999,** *60,* 145–148.

[24] Wineland, D.J.; Monroe, C.; Itano, W.M.; Leibfried, D.; King, B.E.; Meekhof, D.M. *J. Res. Natl. Inst. Stand. Technol*. **1998,** *103,* 259–328.

[25] Leibfried, D.; Knill, E.; Ospelkaus, C.; Wineland, D.J. *Phys. Rev. A* **2007,** *76,* 032324.

[26] Sørensen, A.; Mølmer, K. *Phys. Rev. A* **2000,** *62,* 022311.

[27] Schmidt-Kaler, F.; Hafner, H.; Riebe, M.; Gulde, S.; Lancaster, G.P.T.; Deuschle, T.; Becher, C.; Roos, C.F.; Eschner, J.; Blatt, R. *Nature* **2003,** *422,* 408–411.

[28] Chuang, I.L.; Yamamoto, Y. *Phys. Rev. A* **1995,** *52,* 3489–3496.

[29] Chuang, I.L.; Yamamoto, Y. *Phys. Rev. Lett*. **1996,** *76,* 4281–4284.

[30] Sun, Y.; Hillery, M.; Bergou, J.A. *Phys. Rev. A* **2001,** *64,* 022311; Bergou, J.A.; Hillery, M.; Sun, Y. *J. Mod. Opt*. **2000,** *47,* 487–497.

[31] Reck, M.; Zeilinger, A. *Phys. Rev. Lett*. **1994,** *73,* 58–61.

[32] Zukowski, M.; Zeilinger, A.; Horne, M.A. *Phys. Rev. A* **1997,** *55,* 2564–2579.

[33] Barnett, S.M.; Croke, S. *Adv. Opt. Photon*. **2009,** *1,* 238–278.

Appendix 1. Proof of Lemma 1 in [13]

In order to understand the procedure used to choose the elements in the decomposition of U (6), we use the constructive proof of Lemma 1 in [13]. According to that lemma, it is always possible to write

$$O_A \otimes O_B \exp(\mathrm{i}\zeta)|\varphi_k\rangle = |\Phi_k\rangle, \tag{26}$$

where $\{|\phi_k\rangle\}$ is any maximally entangled basis, ζ_k are some appropriate phases and O_A and O_B local unitaries.

For the proof of (26) let us consider some properties of the concurrence.

(i) A state $|\phi\rangle$ written in the magic basis, is maximally entangled if and only if its coefficients are real, except for a global phase.
(ii) A state $|\phi\rangle$ written in the magic basis, is completely disentangled, i.e. a product state, if and only if the sum of the squares of its expansion coefficients is zero.

According to these two properties if $|\phi\rangle$ and $|\phi^{\perp}\rangle$ are real in the magic basis (and therefore they are maximally entangled), then the state $|\phi\rangle \pm \mathrm{i}|\phi^{\perp}\rangle$ is a product state.

Thus, we can always write $|\varphi_k\rangle = \exp(\gamma_k)|\overline{\varphi}_k\rangle$, where $|\overline{\varphi}_k\rangle$ is real in the magic basis. Likewise we can consider two different states $|\overline{\varphi}_k\rangle$ and $|\overline{\varphi}_l\rangle$, then the combination $2^{-1/2}(|\overline{\varphi}_k\rangle + \mathrm{i}|\overline{\varphi}_l\rangle) = |e,f\rangle$ and $2^{-1/2}(|\overline{\varphi}_k\rangle - \mathrm{i}|\overline{\varphi}_l\rangle) = |e^{\perp},f^{\perp}\rangle$ are product states. Thus, we write

$$\begin{aligned} |\overline{\varphi}_1\rangle &= \frac{1}{2^{1/2}}(|e,f\rangle + |e^{\perp},f^{\perp}\rangle), \\ |\overline{\varphi}_2\rangle &= \frac{-\mathrm{i}}{2^{1/2}}(|e,f\rangle - |e^{\perp},f^{\perp}\rangle). \end{aligned} \tag{27}$$

Following the above arguments, $|\overline{\varphi}_{3,4}\rangle$ can be written as

$$\begin{aligned} |\overline{\varphi}_3\rangle &= \frac{-\mathrm{i}}{2^{1/2}}(\exp(\mathrm{i}\delta)|e,f^{\perp}\rangle + \exp(-\mathrm{i}\delta)|e^{\perp},f\rangle), \\ |\overline{\varphi}_4\rangle &= \pm\frac{1}{2^{1/2}}(\exp(\mathrm{i}\delta)|e,f^{\perp}\rangle - \exp(-\mathrm{i}\delta)|e^{\perp},f\rangle), \end{aligned} \tag{28}$$

for some δ. Finally, by choosing

$$O_A = |0\rangle\langle e| + |1\rangle\langle e^{\perp}|e^{i\delta}, \tag{29}$$

$$O_B = |0\rangle\langle f| + |1\rangle\langle f^{\perp}|e^{-i\delta}, \tag{30}$$

and the phases ζ_k appropriately, we obtain Equation (26)

Appendix 2. The decomposition of U

In this appendix, we show the derivation of the results following the procedure described in Section 3.

(i) In the first step we obtain $U^{\mathrm{T}}U$ in the magic basis

$$U^{\mathrm{T}}U = \frac{1}{a}\begin{pmatrix} 2-3a & 2\mathrm{i}(2a-1)^{1/2}(1-a)^{1/2} & 0 & 0 \\ 2\mathrm{i}(2a-1)^{1/2}(1-a)^{1/2} & 2-3a & 0 & 0 \\ 0 & 0 & a & 0 \\ 0 & 0 & 0 & a \end{pmatrix}, \tag{31}$$

and its eigensystem. The eigenvalues, $\exp(2\mathrm{i}\epsilon_k)$, are given by

$$\exp(2\mathrm{i}\epsilon_k) = \left\{1, 1, \left(\frac{(1-a)^{1/2} \pm \mathrm{i}(2a-1)^{1/2}}{a^{1/2}}\right)^2\right\}. \tag{32}$$

The eigenstates $\{|\Psi_k\rangle\}$ are

$$\begin{aligned} |\Psi_1\rangle &= |\Phi_3\rangle = \frac{\mathrm{i}}{2^{1/2}}(|01\rangle + |10\rangle), \\ |\Psi_2\rangle &= |\Phi_4\rangle = \frac{1}{2^{1/2}}(|01\rangle - |10\rangle), \\ |\Psi_3\rangle &= \frac{1}{2^{1/2}}(|\Phi_1\rangle + |\Phi_2\rangle) \\ &= \frac{1}{2^{1/2}}\left(\frac{1+\mathrm{i}}{2^{1/2}}|00\rangle + \frac{1-\mathrm{i}}{2^{1/2}}|11\rangle\right), \\ |\Psi_4\rangle &= \frac{1}{2^{1/2}}(|\Phi_1\rangle - |\Phi_2\rangle) \\ &= \frac{-\mathrm{i}}{2^{1/2}}\left(\frac{1+\mathrm{i}}{2^{1/2}}|00\rangle - \frac{1-\mathrm{i}}{2^{1/2}}|11\rangle\right). \end{aligned} \tag{33}$$

This set of states is a maximally entangled basis.

(ii) Then, we choose V_A, V_B and the phases ξ_k by Lemma 1. Since $|\Psi_k\rangle$ is real in the magic basis, we can find by comparison of (27) and (28) with (33): $\exp(\mathrm{i}\delta) = \exp[\mathrm{i}(\pi/4)] = (1+\mathrm{i})/2^{1/2}$, and $|e\rangle = |0\rangle$, $|f\rangle = |1\rangle$, therefore

$$V_A = |0\rangle\langle 0| + \exp\left(\mathrm{i}\frac{\pi}{4}\right)|1\rangle\langle 1|, \tag{34}$$

$$V_B = |0\rangle\langle 1| + \exp\left(-\mathrm{i}\frac{\pi}{4}\right)|1\rangle\langle 0|, \tag{35}$$

and the phases ξ_k are easily found to be $\{\exp(\mathrm{i}\xi_1) = -\mathrm{i}, \exp(\mathrm{i}\xi_2) = \mathrm{i}, \exp(\mathrm{i}\xi_3) = \mathrm{i}, \exp(\mathrm{i}\xi_4) = -\mathrm{i}\}$.

(iii) In the next step we calculate a second maximally entangled basis $\{|\widetilde{\Psi}\rangle\}$. It is easy to show that in our case $|\widetilde{\Psi}_k\rangle = |\Psi_k\rangle$.

(iv) We apply the operator U given by Equation (6) to $|\Psi_k\rangle$, getting

$$\begin{aligned} U|\Psi\rangle &= (U_A \otimes U_B)U_d(V_A \otimes V_B)|\Psi_k\rangle, \\ \exp(\mathrm{i}\epsilon_k)|\widetilde{\Psi}_k\rangle &= (U_A \otimes U_B)(\exp(-\mathrm{i}\lambda_k)|\Phi_k\rangle\langle\Phi_k|)(V_A \otimes V_B)|\Psi_k\rangle, \\ \exp(\mathrm{i}\epsilon_k)|\Psi\rangle &= (U_A \otimes U_B)\exp(-\mathrm{i}\lambda_k)|\Phi_k\rangle\langle\Phi_k|\exp(-\mathrm{i}\xi_k)|\Phi_k\rangle, \\ \exp(\mathrm{i}\epsilon_k)|\Psi\rangle &= (U_A \otimes U_B)\exp(-\mathrm{i}\lambda_k)\exp(-\mathrm{i}\xi_k)|\Phi_k\rangle, \end{aligned} \tag{36}$$

where in the last three steps we used Equations (10), (12) and (13). The above equation can also be written as

$$(U_A^{\dagger} \otimes U_B^{\dagger})\exp(\mathrm{i}\lambda_k)\exp(\mathrm{i}\xi_k)\exp(\mathrm{i}\epsilon_k)|\Psi\rangle = |\Phi_k\rangle. \tag{37}$$

Now, similarly to step two, we can choose the operators U_A, U_B, and the phases λ_k, getting

$$U_A = |0\rangle\langle 0| + \exp\left(-\mathrm{i}\frac{\pi}{4}\right)|1\rangle\langle 1|, \tag{38}$$

$$U_B = \exp\left(\mathrm{i}\frac{\pi}{4}\right)|0\rangle\langle 1| + |1\rangle\langle 0|, \tag{39}$$

and the phases λ_k, which are given in Equations (16).